

Article

The Effect of Void on the

Firstname Lastname^{1,†,‡}, Firstname Lastname^{1,‡} and Firstname Lastname^{2,*}

¹ School of Mechanical and Electronical Engineering, Lanzhou University of Technology, Lanzhou 730050, China; e-mail@e-mail.com

² Affiliation 2; e-mail@e-mail.com

* Correspondence: e-mail@e-mail.com; Tel.: +x-xxx-xxx-xxxx

† Current address: Affiliation 3

‡ These authors contributed equally to this work.

Version October 4, 2018 submitted to Journal Not Specified

Abstract: Fracture processes of nanocrystalline metallic materia is affected by dislocation, nanovoid and other defects. Existing studies of defect evolution in titanium-aluminium alloy cover the case that voids located in single crystals, inside grain in poly crystals and at the grain boundaries. Molecular dynamics simulation was performed to study the evolution of a spherical nanovoid in $\alpha+\gamma$ two-phase titanium-aluminium alloy under uniaxial tension. The results show that voids located at the α/γ phase boundary have significant detract to strength of Ti-Al polycrystalline.

Keywords: $\alpha + \gamma$ two phase TiAl alloy; void; molecular dynamics

1. Introduction

TiAl alloy has been used as structural material in aviation industry because its inherent advantages such as low density and self-diffusion rates, high elastic module and high strength [1]. Two-phase titanium aluminum alloys with proper phase distribution and grain size exhibit better mechanical performance compared with monolithic constituents $\gamma(\text{TiAl})$ and $\gamma(\text{Ti}_3\text{Al})$ alloy [2]. Brittle fracture in TiAl alloy strongly affects the safety of fracture of structure like turbo of aircraft engine and combustion generator.

Deformation phenomena in TiAl alloys have been widely studied in order to overcome the problems associated with the limited ductility and damage tolerance. The literature data covers a wide range of parameters such as alloy composition, microstructure and deformation temperature. Much of the work has been performed on single phase γ alloys and PST crystals. Rupture failure at the macroscopic scale can be attributed to nucleation, growth and propagation of cracks, but at the microscopic scale cracks are initially easily formed at defects in the casting process, such as voids and inclusions [3]. These defects are known to play a fundamental role in the deformation of the material. Nucleation, growth and coalescence of voids are deemed as the primary mechanism of ductile material fracture, in which void growth is particularly important. Therefore, it is necessary to study the deformation response of porous materials with the consideration of microstructure evolution.

Brittle fracture in TiAl alloy strongly affects the safety of fracture of structure like turbo of aircraft engine and combustion generator [3]. Defects such as grainboundary, void and segregation plays an significant role in the process of fracture [3]. In order to understanding the mechanism of brittle fracture, multi-scale methods from micro to marco scale have been applied to investigate the behavior of fracture. It's necessary to carefully examine the revolution of defects and its influence on the fracture process at atomic scale. A previous study on void growth in gamma-TiAl single crystal has reveals that void with high volume fraction detracts incipient yield strength [3]. Molecular dynamics(MD method has been use to investigate the evolution of void in materials in nanoscale [3]. The fracture mechanisms

33 in the duplex micro-structure are plasticity induced grain boundary decohesion and cleavage, while
 34 those in the lamellar microstructure are interface delamination and cracking across the lamellae [].

35 MD simulations has reveals that existence of voids alone may contribute to strain hardening
 36 because they are barriers to dislocation movement [3]

37 2. Molecular Dynamics Simulation

38 2.1. Atomic Potential

39 The interaction of particle in the material is determined by interatomic potential. Many reported
 40 examples of crack propagation in metal materials were performed with embedded atomic method
 41 due to is better accuracy in metal lattice compare with F-S and L/J []. The embedded atom method
 42 (MEAM) potential developed by Zope and Mishin by [] was used in the study. The simulation is
 43 submitted by MD simulations with the Large-scale Atomic/Molecular Massively Parallel Simulator
 44 (LAMMPS) open-source code []. We performed constant-pressure and constant-temperature (NPT)
 45 molecular dynamics simulation.

$$E_{total} = \sum F_i(\rho_{h,i}) + \frac{1}{2} \sum_i \sum_{j(\neq i)} \phi_{ij}(R_{ij}) \quad (1)$$

46 where E_{total} is the total energy of the system, $\rho_{h,i}$, is the host electron density at atom i due to the
 47 remaining atoms of the system, $F_i(\rho)$ is the energy for embedding atom i into the background electron
 48 density ρ , and $\phi_{ij}(R_{ij})$ is the core-core pair repulsion between atoms i and j separated by the distance
 49 R_{ij} . It can be noted that F_i only depends on the element of atom i and ϕ_{ij} only depends on the elements
 50 of atoms i and j . The electron density is, as stated above, approximated by the superposition of atomic
 51 densities, namely

52 2.2. Model Creation of Crystalline

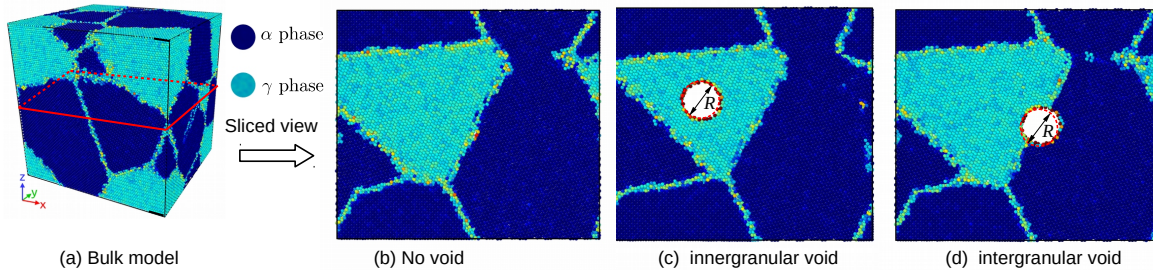


Figure 1. Overview of model creation

53 [] γ TiAl has a fcc-centered tetragonal with an $L1_0$ structure [], and α TiAl is hcp structure, the
 54 structure of the two initial cells are shown in Fig.[], and the constructing parameters are given by Table.[].
 55 The simulation cells of two phase polycrystalline with an initially spherical void at different position
 56 are shown in figure []. Periodic boundary conditions (PBC) are applied along all three directions, that
 57 makes poly crystal with periodic nanovoid structures. The initial dimension of simulation cell is $L_x =$
 58 nm, $L_y =$ nm, $L_z =$ nm, and each model contains about 4.6 million atoms. The grain orientation and
 59 size were randomly created with Voronoi method with code ATOMSK [], and resulting in the arbitrary
 60 shape and orientation of the grains. Only one spherical void defect was placed intragranularly or
 61 intergranularly within each simulation model void within each simulation model. The intragranular
 62 spherical void was located in grain interior of the largest grain of the simulation model, as shown in
 63 Fig. []. The intergranular spherical void was at the center of the simulation cell, as shown in Fig. [].

Table 1. Parameters of nanocrystalline

Phase	Space group	Designation	Parameters
α_2	P6 ₃ /mmc	0 ₁₉	$a = 0.5765$ $c = 0.46833$
γ	tP4	L1 ₀	$a = 0.3997$ $c = 0.4062$

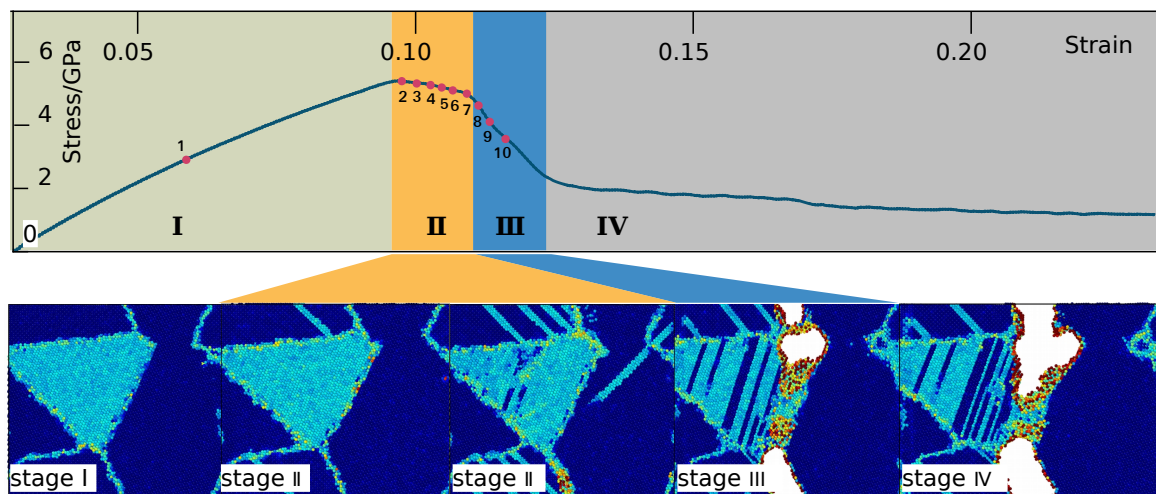
64 **2.3. Analysis method**

The centrosymmetry parameter is defined as follow:

$$P = \sum_{i=1}^6 |\vec{R}_i + \vec{R}_{i+6}|^2 \quad (2)$$

65 where \vec{R}_i and \vec{R}_{i+6} are the vectors corresponding to the six pairs of opposite nearest neighbors
 66 in the fcc lattice. The centrosymmetry parameter(CSP) is zero for atoms in a perfect lattice. In other
 67 words, if the lattice is distorted the value of P will not be zero. Instead, the parameter will have a value
 68 within the range corresponding to a particular defect. By removing all the perfect and surface atoms
 69 within the bulk, the existence of dislocation atoms become visible.

70 **3. Results and Discussion**

**Figure 2.** perfect-line2-2**Table 2.** Key point during tensile process

Key Number	1	2	3	4	5	6	7	8	9	10
Time/ps	0	0.15	0.16	0.17	0.18	0.19	0.20	0.21	0.22	0.23
Strain	0	0.15	0.16	0.17	0.18	0.19	0.20	0.21	0.22	0.23

71 **3.1. Deformation Behaviour of Two Phase Alloys without Void Defects**

72 However, the following discussion concentrates on deformation phenomena that rely on the
 73 elastoplastic codeformation of the γ and γ_2 phases and on the particular point defect situation occurring
 74 in twophase alloys. Due to this effect ($\alpha_2 + \gamma$) alloys exhibit some remarkable properties that are

unlike those of either constituent. The configure of atoms is shown in Fig.8, it can be seen that

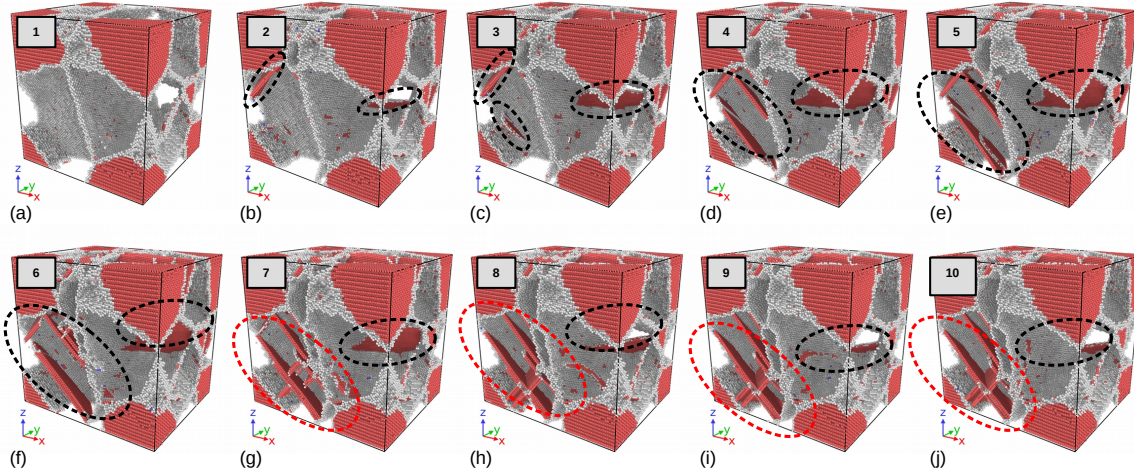


Figure 3. γ phase deformation

dislocation emission initiate in γ phase in XXX ps, and the deformation can be mainly confined to the majority γ phase. $\gamma(\text{TiAl})$ deforms by octahedral glide of ordinary dislocations with the Burgers vector $b=1/2<110]$ and superdislocations with the Burgers vectors $b=<101]$ and $b=1/2 < 11\bar{2}]$. The other potential deformation mode is mechanical twinning along $1/6 < 11\bar{2}]111$. From Fig.8, of the two constituents of $(\alpha_2+\gamma)$ alloys, the α_2 phase is more difficult to deform. A reason for the unequal strain partitioning between the α_2 and γ phase is certainly the strong plastic anisotropy of the α_2 phase. TEM examinations performed on tensile tested lamellar alloys have revealed that the limited plasticity of the α_2 phase is mainly carried by local slip of $<\text{a}>$ -type dislocations with the Burgers vector $b = 1/3 < 11\bar{2}0 >$ prism planes⁸, which is by far the easiest slip system in α_2 single crystals. Basic

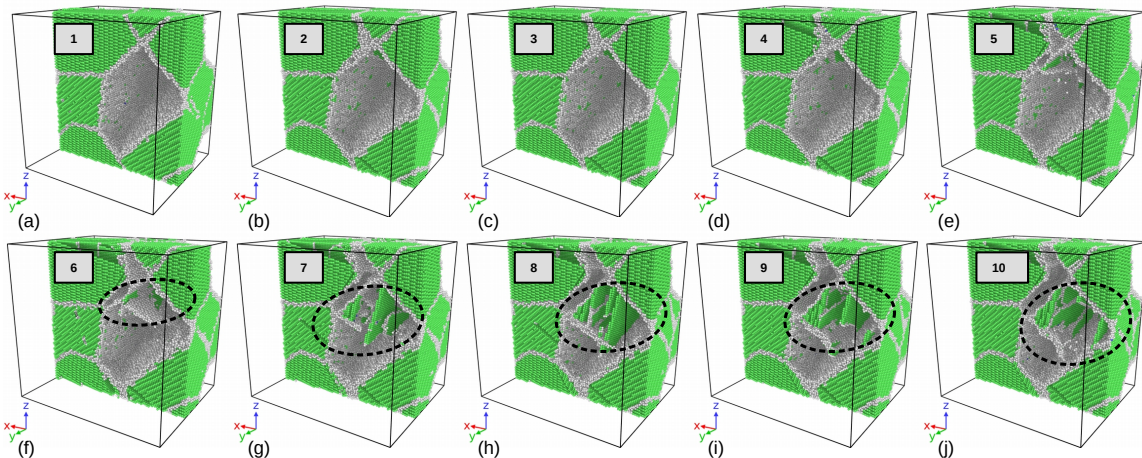


Figure 4. α phase deformation

deformation mechanism of α phase

1. In many cases the orientation of slip is changed because the crystallographically available slip and directions are not continuous across the interface. This may significantly reduce the Schmid factor and thus impede slip transfer. At the γ/γ interfaces the orientation of the slip plane could change through a relatively large angle of about 90 degree. Reorientation of slip is always required at the α_2/γ interface; the smallest angle between the corresponding slip planes 111_γ and $10 - 10_{\alpha_2}$ is about 19 degree [1].

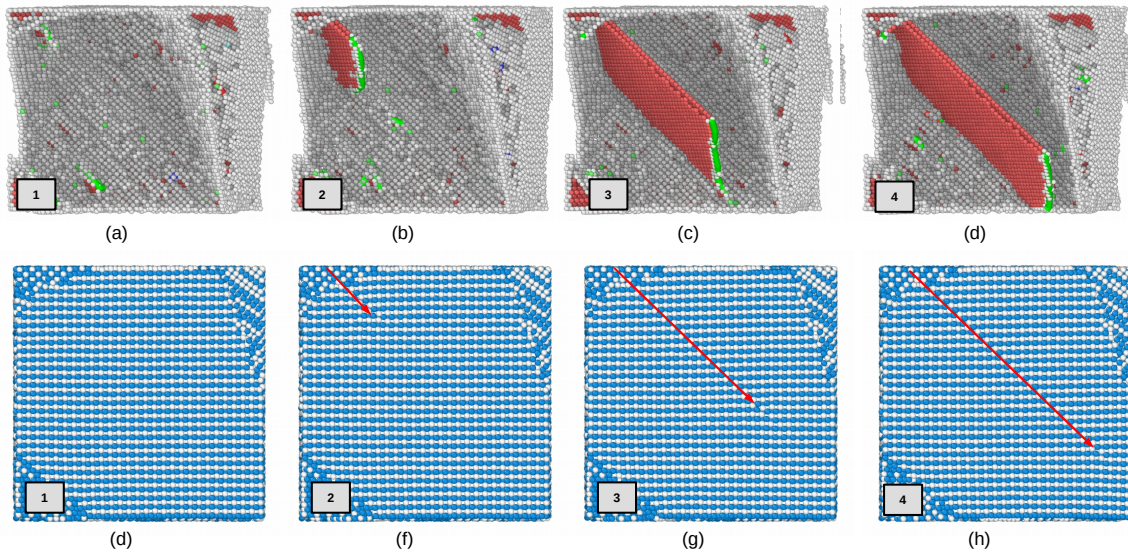


Figure 5. Dislocation in γ

92 The core of a dislocation intersecting an interface often needs to be transformed. For example, an
 93 ordinary $1/2<110]$ dislocation gliding in one γ grain has to be converted in to a $<101]$ super dislocation
 94 with the double Burgers vector gliding in an adjacent γ grain. At the α/γ interface the dislocations
 95 existing in the $D0_{19}$ structure have to be transformed into dislocations consistent with the $L1_0$ structure.
 96 These core transformations are associated with a change of the dislocation line energy because the
 97 lengths of the Burgers vectors and the shear module are different.

98 Dislocations crossing semi-coherent boundaries have to intersect the misfit dislocations, a process
 99 that involves elastic interaction, jog formation and the incorporation of gliding dislocations into the
 100 mismatch structure of the interface. When the slip is forced to cross α_2 lamella, pyramidal slip of the α_2
 101 phase is required, which needs an extremely high shear stress.

102 *3.2. Evolution of spherical void in the simulation with intragranular spherical voids*

103 The volume defects considered pertain to three-dimensional objects contained within a matrix.
 104 Three-dimensional structures composed of zero-, one- or two-dimensional defects are not considered
 105 here. Second-phase particles, precipitated within, as a consequence of a thermal treatment, or taken
 106 up, as a consequence of a material processing route, into a matrix of the first, dominant phase, disrupt,
 107 more or less (as possibly associated with the occurrence of incoherent or coherent interfaces; see Sect.
 108 5.3), the long-range translation symmetry of the matrix. They may induce considerable misfit-stress
 109 fields and thus can influence material properties pronouncedly. Such stress fields surrounding the
 110 second-phase particles can be due to misfit between the volume occupied by the second-phase particle
 111 when unconstrained and the space ("hole") put at its disposal by the matrix. Such misfit can arise
 112 due to specific volume differences induced by precipitation or by different thermal expansion or
 113 shrinkage upon heating or cooling the specimen. A possibly favourable effect of second-phase particles
 114 is a contribution to the enhancement of mechanical strength. Considering yielding of a material as
 115 related to glide of dislocations (Sect. 5.2.5), any mechanism obstructing dislocation glide improves the
 116 mechanical strength. In the discussion of the Frank-Read source for dislocation (-line) production (Sect.
 117 5.2.6) it was made clear that second-phase particles can serve as obstacles for dislocation migration:
 118 the stress fields surrounding the second-phase particles can be of "antagonistic" nature and "block"
 119 propagation of the stress field of a migrating dislocation: the second-phase particle acts as "pinning
 120 point". It was already indicated that in order that a dislocation can pass two pinning points (A and B
 121 in Fig. 5.13; see Sect. 5.2.6) a critical shear stress is needed that depends on the distance between the
 122 obstacles (which can be second-phase particles):

$$\tau_0 = Gb/d \quad (3)$$

where d represents the distance between A and B and thus reflects the dependence of the critical shear stress τ_0 on the second-phase particle density and distribution. This mechanism for hardening is designated as the Orowan process (with τ_0 as the Orowan (shear) stress ; see also Sect. 11.14.4). As a result of the Orowan process, upon passage of the pinning points by a series of gliding dislocations, a system of concentric loops is formed around the second-phase particles (see Fig. 5.27). Consequently, the effective average distance between the second-phase particles has decreased to d which implies a necessary increase of the value of critical shear stress required for continuation of dislocation glide (cf. (5.10)). A step, of the width of a burgers vector, will be generated at both sides of a crystal along the direction of the burgers vector after dislocation traversing the entire crystal, as is shown in ???. A small step will be formed at spherical void surface toward the void interior after dislocation absorption at spherical void surfaces, as is shown in ???. If a great number of dislocation slip along their respective systems towards the spherical nanovoid in all directions, and are absorbed at spherical void surfaces, the spherical nanovoid will eventually shrink from the dash circle to

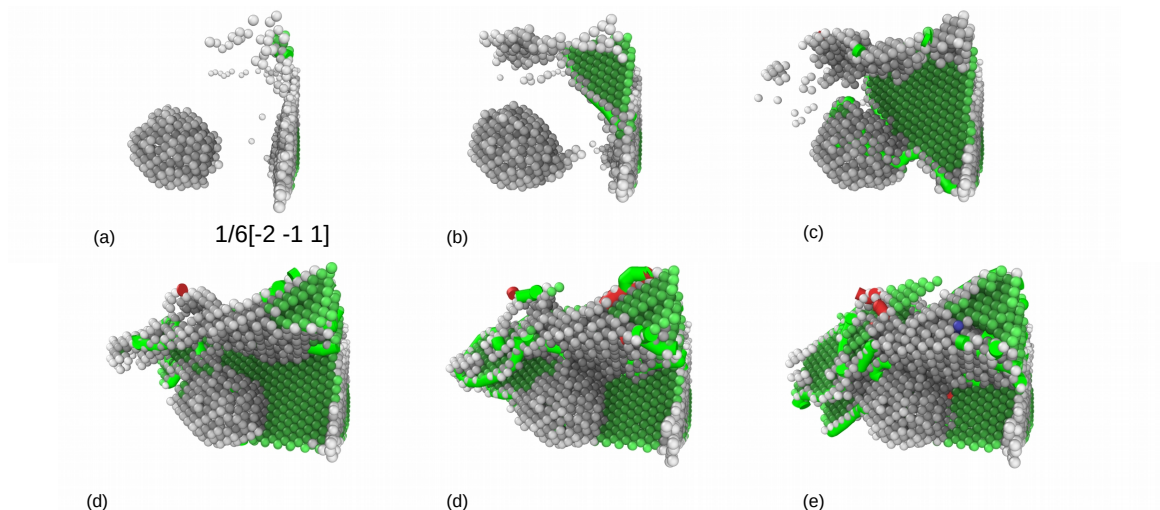


Figure 6. Dislocation around void

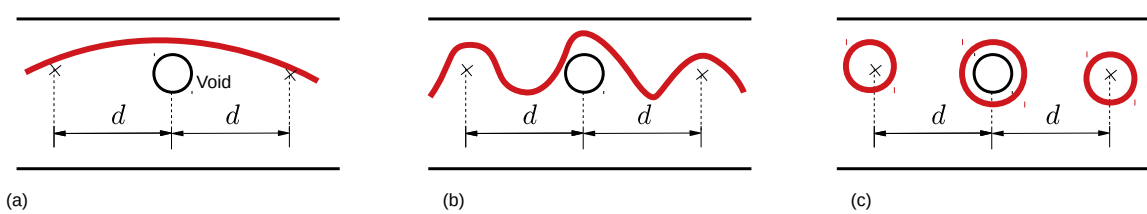


Figure 7. orowan

3.3. The effect of void on the strength of material

Void of R=10 was placed at phase boundary, inside α phase grain respectively. Effect of void at different position under uniaxial tension is shown in Fig.9. The strength of materials with void in different size and at different position is shown in Fig.9. The results show that the model without void defect has best strength, while the void located inside α phase detracts the strength of the material most, and the void at the phase boundary have less impact on the strength.

The effect of size is expectable that the greater voids detracts the strength of the materials more, however, it has been observed in the simulation that there is a critical value about 15A for voids at

¹⁴⁴ different position. The voids larger than 15 Å have dramatic detraction to the strength of the material.
¹⁴⁵ Conventional definition of strength of materials with geometry subtraction was applied to the model,
¹⁴⁶ and theoretical strength of the models was calculated by formulation 4:

$$\sigma^* = \sigma_0 \cdot \frac{A^*}{A_0} \quad (4)$$

¹⁴⁷ where σ_0 is the strength of the model without void defects 5.26 Gpa, and A_0 is initial section area,
¹⁴⁸ $A = a \times b = 36000 A^2$, A^* is section area in consider of the subsection that results from the voids.
¹⁴⁹ Comparing with the strength determined by molecular dynamics simulation and the results calculated
¹⁵⁰ with formulation 4, it can be assumed that the main factor that affects the strength of materials can be
¹⁵¹ attributed to local behaviour of the materials, thus revolution of defects should be examined carefully.

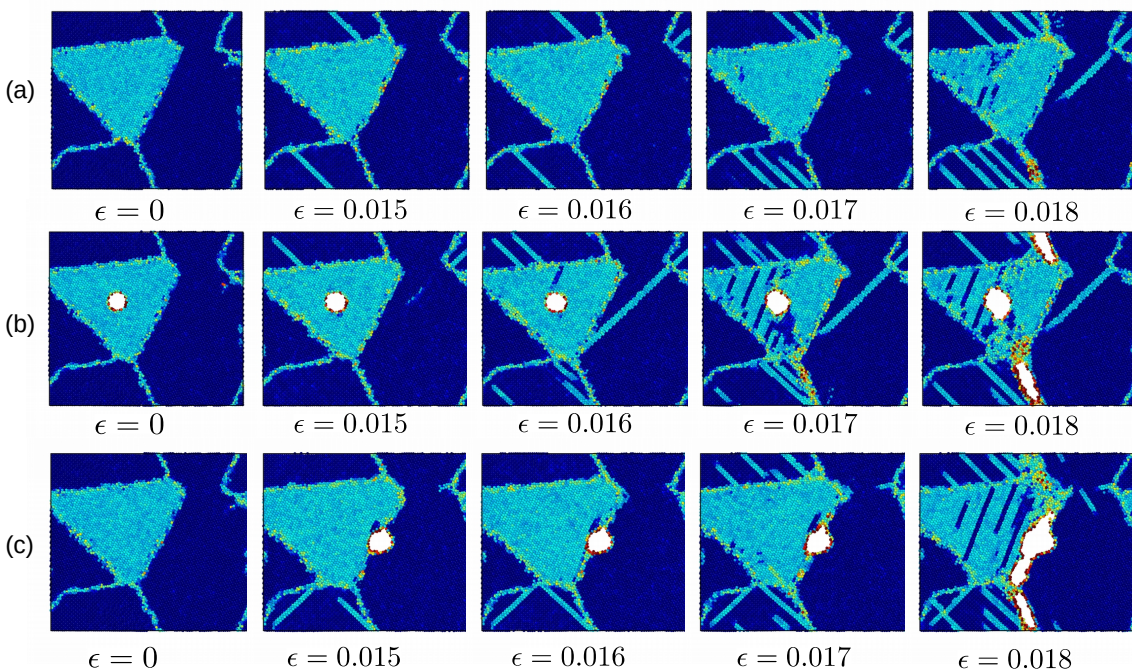


Figure 8. Yield process of the models

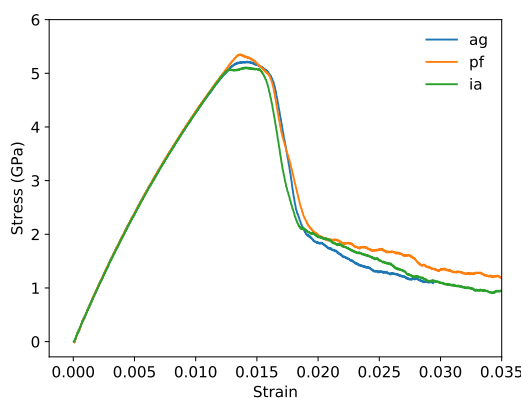


Figure 9. Stress-Strain

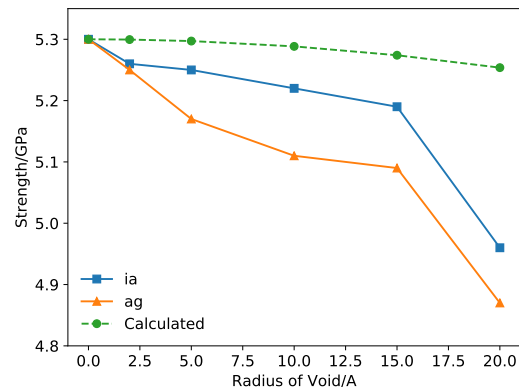


Figure 10. Strength of models

Voids with different size: 2Å, 5Å, 10Å, 15Å were placed into the model respectively. It has been observed that voids detracts the strengths of the material. The max stress stress of the simulation cell

decreases as the volume of voids are lareger. From Fig ??, there is a critical value of void radius about 15A, the void greater than 15A cause serious detraction of strength of material. Engineering stress is calculated

$$\sigma = S / A$$

152 The rate of decrease of loading area are smaller comparing with the detraction of strength, so it can
153 be assumed that the yield yield behaviour and strength is much more related with local behaviour of
154 grain boundaries and void.

155 Grain and phase boundaris are obstnacles to deformation process, thus the stability of boundaries
156 have great impact on the strength of materials. Interactive between grainboundary and void determines
157 the fracture mode of the TiAl alloy.

According to Schmid's law:

$$\tau = \sigma * m$$

where m is the Schmid factor :

$$m = \cos(\phi)\cos(\lambda)$$

158

159 References

- 160 1. Vu, T.T.T.; Zehender, T.; Verheijen, M.A.; Plissard, S.R.; Immink, G.W.G.; Haverkort, J.E.M.; Bakkers,
161 E.P.A.M. High optical quality single crystal phase wurtzite and zincblende InP nanowires. *Nanotechnology*
162 **2013**, *24*, 115705. doi:10.1088/0957-4484/24/11/115705.
- 163 2. Kim, Y.W. Effects of microstructure on the deformation and fracture of γ -TiAl alloys. *Materials Science and*
164 *Engineering: A* **1995**, *192-193*, 519–533. doi:10.1016/0921-5093(94)03271-8.
- 165 3. Xiong, L.; Xu, S.; McDowell, D.L.; Chen, Y. Concurrent atomistic-continuum simulations of dislocation-void
166 interactions in fcc crystals. *International Journal of Plasticity* **2015**, *65*, 33–42. doi:10.1016/j.ijplas.2014.08.002.

167 © 2018 by the authors. Submitted to *Journal Not Specified* for possible open access
168 publication under the terms and conditions of the Creative Commons Attribution (CC BY) license
169 (<http://creativecommons.org/licenses/by/4.0/>).